Characterization of Electrical and Mechanical Properties for Coaxial Nanofibers with Poly(ethylene oxide) (PEO) Core and Multiwalled Carbon Nanotube/PEO Sheath

Satyajeet S. Ojha,[†] Derrick R. Stevens,[‡] Kelly Stano,[†] Torissa Hoffman,[‡] Laura I. Clarke,[‡] and Russell E. Gorga*[,†,§]

Department of Textile Engineering, Chemistry, and Science, Department of Physics, and Fiber and Polymer Science Program, North Carolina State University, Raleigh, North Carolina 27695

Received November 27, 2007; Revised Manuscript Received January 16, 2008

ABSTRACT: The present work focuses on the electrical and mechanical characterization of nanocomposite fibers having core−sheath (or bicomponent) morphologies. Owing to their unique mechanical and electrical properties, multiwalled carbon nanotubes (MWNTs) have been utilized in the nanocomposite construction. Submicron diameter nanofibers (200–300 nm) with core−sheath morphology were fabricated from a polymer/MWNT solution and collected in random mats. By constraining the MWNTs to the sheath, significant increases in the mechanical properties were observed at lower MWNT concentrations when compared to mats made from single-layer fibers. The electrical properties of the core−sheath mats showed similar gains, having a critical weight percent more than 10 times lower than that of the single-layer mats.

Introduction

With superior electrical and mechanical properties, as well as very high aspect ratios (>1000), carbon nanotubes (CNTs) are well-suited for polymer composites.[1−4] Specifically, much interest has been generated in the fabrication of nanocomposite fibers reinforced with CNTs.[5−11] To fully realize the potential of nanocomposites (films, fibrous mats, etc.), a comprehensive understanding of how the composite morphology affects the physical properties is needed. The work presented here focuses on the comparison and possible advantages of core−sheath nanofibers to single-layer nanofibers.

Electrospinning is a simple technique used to generate fibers with submicrometer diameters. With this procedure electrostatic forces, not mechanical, are responsible for the fiber production.[12] A pendant polymer solution droplet, typically conical in shape, is charged until the static repulsion overcomes surface tension, resulting in a highly extensional flow. As a consequence, ultrahigh drawing of fibers takes place and exceedingly fine fibers are produced.[5−13] These nanofibers have very high surface area to volume ratios which make them ideal candidates for tissue engineering,[14] conductive nanowires,[15] supercapacitors,[16] nanosensors,[17] filtration membranes,[18,19] and many other applications. Specifically, nanofibers having a core−sheath structure could be applied to tasks such as sustained delivery of drugs[20] or the preservation of a biological agent from an externally aggressive environment.[21]

Fabrication of coaxial or core−sheath nanofibers is realized by injecting polymer solutions or melts through two annular orifices into a region of uniform electric field. Such a technique to produce coaxial nanofibers is advantageous when one polymer component is incapable of forming nanofibers due to its inherent fluid characteristics. Morphology of these nanofibers depends on factors such as viscosity, shear stresses, bending stability, and Maxwell stresses. These properties should be the same or similar for each of the two polymers used in coaxial electrospinning.

Typical of a composite material, changes in the dopant level (MWNTs in this case) will alter some physical properties, such as conductance, via a percolating process.[22] As the MWNT concentration is increased, nanotube clusters develop within the insulating matrix. At a critical weight percentage these conductive networks form a complete path across the sample, transforming the composite from insulating to conducting. This percolation threshold is dependent on factors such as nanotube/polymer interaction and composite morphology. Similarly, we expect to see an increase in mechanical properties with nanotube loading until a concentration where sufficient aggregation occurs, and there is a resulting decrease in modulus and strength due to insufficient load transfer and stress concentrators, respectively.

The core−sheath morphology provides a unique template to develop and improve technologies while furthering the view of percolation in polymer composites. CNT composites have a wide range of percolation thresholds depending on their specific composition.[23−27] Single-layer fibers of polymer/MWNT composites have been previously reported with critical weight percents <1% for both single fibers and mats.[4,28] This is quite advantageous from a production point of view as CNTs are still an expensive material. By using core−sheath fibers and confining the CNTs to the sheath, this weight percent may be altered even further. Previous research has shown a high dependence of the critical weight percent on such factors such as nanotube aspect ratio, orientation angle, and dopant homogeneity,[29,30] with this work occurring mostly in films. The information gathered from studying mats of core−sheath fibers will help to complete the developing picture of how the structure of the sample itself (sample morphology) affects these factors to aid or hinder the percolation process.

In this work, coaxial nanofibers having pure PEO as the core and PEO doped with different concentrations of MWNTs in the sheath are produced. Since the electrospinning process is very fast, the two jets of polymers do not mix,[31] and discrete layers with and without MWNTs remain. The electrical and mechanical properties of coaxial nanofibers are characterized, and the resulting properties are compared to that of single-layer fibers.

* To whom correspondence should be addressed.
[†] Department of Textile Engineering, Chemistry, and Science.
[‡] Department of Physics.
[§] Fiber and Polymer Science Program.

10.1021/ma702634a CCC: $40.75
Published on Web 02/22/2008

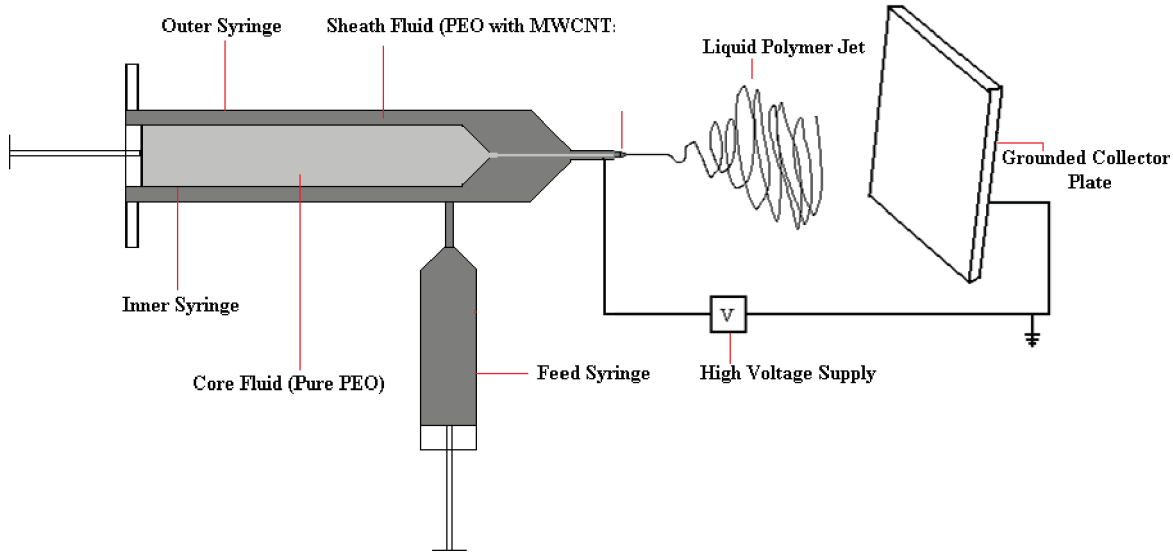

Figure 1. Electrospinning setup used in core−sheath fabrication.

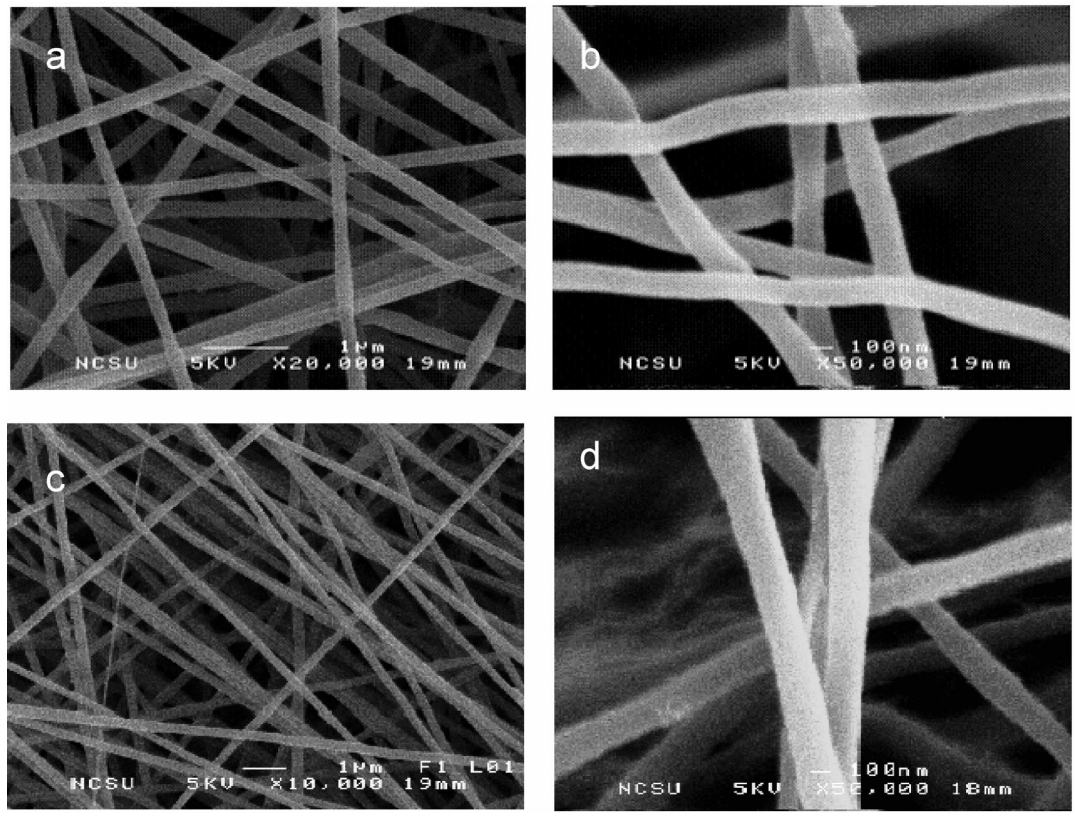

Figure 2. Scanning electron images of single-layer nanofibers (a, b) and core−sheath nanofibers (c, d).

Experimental Section

Materials. Poly(ethylene oxide) (PEO) of M_w 900 000 was obtained from Scientific Polymer Products. The concentration of PEO in water was 4 wt %. MWNTs supplied by Nano-Lab were produced by plasma-enhanced chemical vapor deposition (CVD) using acetylene and ammonia with an iron-based catalyst and were grown on mesoporous silica substrate.[32] The diameter and length of these nanotubes were 15 ± 5 nm and 5–20 μm, respectively, with 95% purity. MWNT were dispersed in deionized water using Ultrasonic model 2000U generator and probe operating at 25 Hz for 1 h. Gum Arabic was used at a constant concentration of 3 wt % (relative to the concentration of PEO) to aid dispersion in all samples. Concentration of MWNT was varied from 0.1 to 3.0 wt %. Core fluid (pure PEO) was stained with bromophenol.

Electrospinning Equipment. Electrospinning was performed using two perpendicularly placed programmable syringe pumps (New Era NE 500). The combined feed rate for both the core and sheath components was 50 μL/min (which is controlled by the pump pushing the concentric syringes). The distance between the tip and the grounded electrode was kept constant at 15 cm. Two concentric capillaries were used having diameters 16G and 20G for sheath and core fluid, respectively. Figure 1 shows the design of our electrospinning setup.

Characterization Techniques. Morphology of nanofibers obtained from coaxial electrospinning was determined through scan-

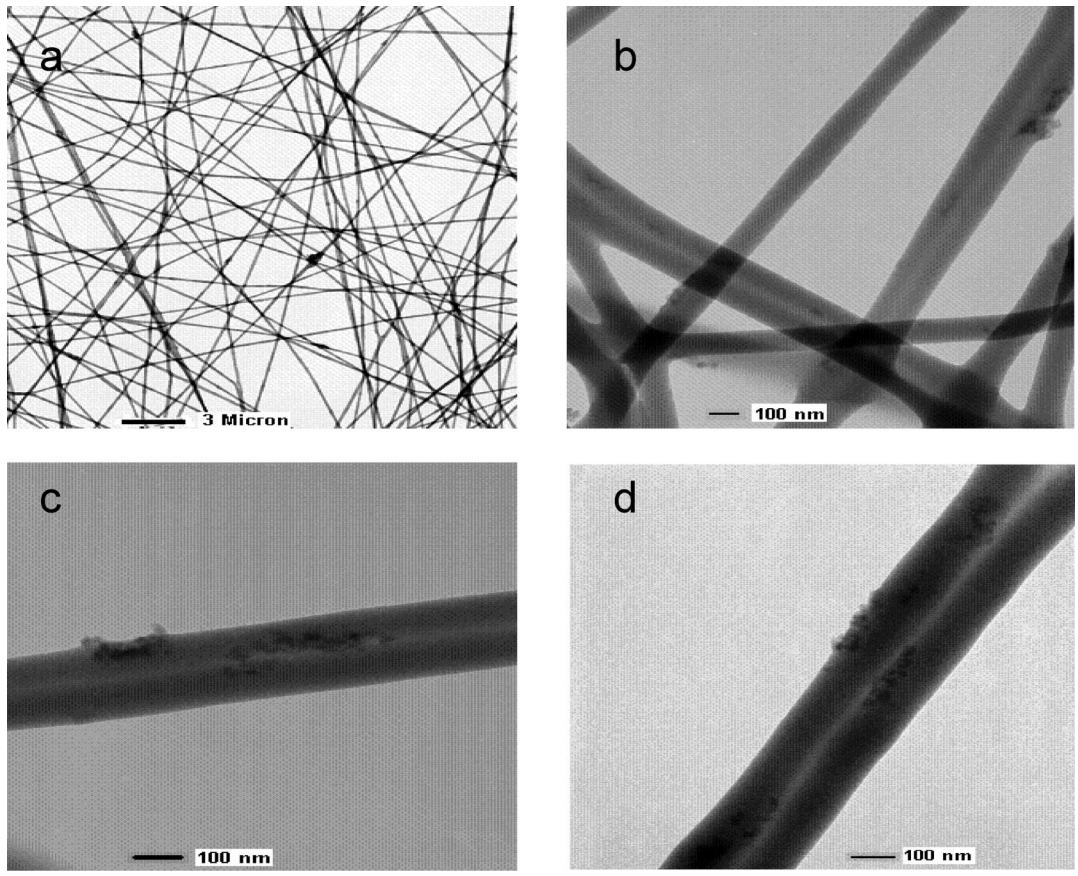

Figure 3. Transmission electron micrographs of PEO (core)/PEO with MWNTs (sheath) core−sheath nanofibers: (a) low magnification of 0.05 wt % MWNTs; (b) 0.05 wt % MWNTs; (c) 0.25 wt % MWNTs; (d) 0.50 wt % MWNTs.

ning electron microscopy (SEM) using JEOL JSM-6400 FE with energy dispersive X-ray spectroscopy (EDS) operating at 5 kV. Coaxial nanofibers samples were collected on aluminum foil and were sputter-coated by a K-550X sputter coater with Au/Pd having thickness ∼100 Å to reduce charging.

Transmission electron microscopy was performed using FEI/Philips EM 208S operating at 80 kV. The electrospun nanofibers were directly deposited on Cu grids coated with a layer of formar and carbon film.

Electrical measurements were conducted by spinning mats directly on flat interdigitated electrodes (IDEs) with glass substrates. The electrodes are comprised of ∼150 Å of chromium and ∼1150 Å of gold. Each electrode consists of 26 finger pairs with 1 mm long, 10 μm wide digits spaced by 10 μm, and two contact pads of ∼1 mm^2 each. Electrical measurements were carried out using a remote source meter (Keithley, 6430 sub-fA). Electrodes were measured before and after sample deposition, nominally from −10 to 10 V with 0.1 V steps and a 15 s wait time after the application of a voltage change. The sample space was evacuated to ∼1 × 10^{-7} Torr. Use of planar electrodes allowed the reliable measurement of these thin, highly porous mats, where the fringe fields of the electrodes penetrate into the mat.[33] The thickness of the electrospun samples was kept constant, so direct comparisons could be made, by keeping the time and other conditions constant for each mat.

The void volume fraction or porosity of the nanofiber mats was calculated using Image J analyzer. SEM images were scanned through Image J, and layers of nanofibers were differentiated through a gray scale. The fiber length is much greater than the layer thickness in the mats, as determined by the fiber diameter, making them essentially two-dimensional. Hence, the void area in one single layer could be approximated to be the total void volume fraction.

Tensile tests were performed using an Instron model 5544 using the Bluehill version 1.00 software. Samples were prepared according to ASTM standard D4762-04. The gauge length of the mats was 3 cm, and the average thickness was 0.12–0.14 mm. Measurements were done at 70 °F, 65% RH, and a strain rate of 5 mm/min.

Results and Discussion

Morphological Characterization. Scanning electron micrographs show uniform nanofibers with diameter around 200 nm. The overall fibrous mat morphology of the core−sheath nanofibers appears to be no different than that for the single-layer nanofibers from the same polymer (PEO). Figure 2 shows the scanning electron micrographs of single layer (a, b) as well as coaxial (c, d) nanofibrous mats.

In order to investigate and verify the core−sheath morphology of electrospun nanofibers, transmission electron microscopy was utilized. It is evident from Figure 3 that the nanofibers obtained have discernible core of pure polymer (PEO) and sheath of PEO doped with MWNTs. In our previous work we demonstrated that addition of MWNTs has a relatively small effect on the rheology of the polymer solution, and we, therefore, did not expect tremendous differences in the overall mat morphology for the core−sheath fibers.[4] The diameter of the core component was estimated to be about 40–50 nm from analysis of the TEM micrographs. However, since the core and sheath polymers are identical, we expect the interfacial region to relatively broad, and therefore the individual component thicknesses are estimates. At low concentration of nanotubes, relatively good dispersion was achieved, but as the concentration of nanotubes increased, the tendency to aggregate also increased, as seen in the transmission electron micrographs (where for higher loadings more MWNT clusters are observed). It is interesting to note that MWNT aggregation in the core−sheath morphology is more pronounced than that for the single-component system at

Table 1. Comparison of Mechanical Properties of Single-Layer and Core−Sheath Nanofibers

sample	MWNT concn in sheath layer (wt %)	effective MWNT concn (wt %)	tensile strength (MPa)	modulus (MPa)	void volume fraction (%)
pure PEO (single-layer)	0	0	10 ± 0.2	12.3 ± 1.5	75
PEO (single-layer)	0.25	0.25	9.2 ± 0.3	19.6 ± 1.5	75
PEO (single-layer)	1.0	1.0	9.4 ± 0.4	37.7 ± 2.1	75
PEO (single-layer)	3.0	3.0	5.0 ± 0.3	23.6 ± 1.7	75
PEO (core)/PEO w/MWNTs (sheath)	0.1	0.05	3.2 ± 0.4	78.8 ± 1.0	73
PEO (core)/PEO w/MWNTs (sheath)	0.50	0.25	7.6 ± 0.3	182 ± 1.6	74
PEO (core)/PEO w/MWNTs (sheath)	1.0	0.50	5.2 ± 0.2	50.4 ± 0.6	76

comparable MWNT loadings.[4] This is not surprising, and we believe this is due to the confinement of the MWNTs (or the shape of the volume) in the sheath component.

Mechanical Characterization. In order to determine any changes in mechanical properties due to the bicomponent nature of the fibers, tensile testing was performed. To compare the bicomponent fibers to the monocomponent fibers, the MWNT concentration for the core−sheath fibers was corrected to account for the MWNT concentration in the entire fiber (not just the sheath layer). This "effective" concentration is half that for the sheath layer by itself (based on the PEO mass throughput during electrospinning). Tensile tests were performed on three samples having different effective MWNT concentrations (0.05, 0.25, and 0.50 wt %) of MWNTs. The tensile data suggest that the core−sheath structure embrittled the nanofibrous mats. At 0.25 wt % effective MWNT loading, the modulus of the core−sheath structure (182 MPa) is an order of magnitude greater than that for the single-layer system (19.6 MPa), as shown in Table 1. However, the tensile strength for the bicomponent system (7.6 MPa) is slightly less than that for the single-layer system (9.2 MPa). This large change in modulus as a function of the fiber morphology was an extremely unexpected result. In both morphologies (bicomponent and single-layer) the modulus goes through a maximum as a function of nanotube concentration. The increase in modulus is attributed to an increased reinforcement as the concentration of the stiffer component increases. The point at which the modulus decreases (from the maximum) is attributed to nanotube aggregration as concentration increases, which results in less surface area available for load transfer. However, the maximum is shifted to lower concentrations for the bicomponent system, indicating that the nanotubes tend to aggregate at lower concentrations when confined to the sheath layer (in the bicomponent morphology). This is not surprising since we observe more nanotube clusters in the bicomponent structure as the MWNT concentration increases (as discussed above).

Comparing the maximum modulus for both the single- and bicomponent morphologies, it is evident that the maximum in the bicomponent case (182 MPa at 0.25 wt % effective loading) is roughly 5 times the maximum in the single-layer morphology (38 MPA at 1 wt %). There are two ways to interpret this result. One is that the maximum modulus of each morphology is identical, but in the case of the single-layer system, we missed the optimum concentration (either between 0.25 and 1 wt % or between 1 and 3 wt %). However, it seems unlikely that the maximum would reach that in the bicomponent system due to the difference in moduli for both morphologies. Another hypothesis is that the reinforcing effect in the bicomponent morphology is greater than that for the single-layer morphology. Higher rigidity near the fiber surface (as in the bicomponent morphology) could result in a stiffer mat due to an increased stiffness at fiber−fiber junctions (presumably the weak link in the nonwoven structure).

Electrical Characterization. Mats of core−sheath nanofibers, with multiple weight percentages, were spun directly on interdigitated electrodes. Current–voltage curves were measured for each sample. The conductance was calculated from the linear portions of the current–voltage characteristics. Conductance as a function MWNT weight percent was fit to determine the critical weight percent. (The critical weight percent is the inflection point in the percolation curve where the material transitions from insulating to conducting.) For the core−sheath mats the weight percent is reported as one-half of the weight percent used in the sheath during construction. This division by 2 is to better represent the weight percent of the entire fiber by accounting for the core and sheath volumes. In addition, it allows for a better comparison to the single-layer mats. As shown in Figure 4, it is evident that the critical weight percent for the core−sheath fibers is much lower than for the single layer. We point out that this would be true even without adjusting the weight percentage. The data were fit with both a Fournier model[24,34] and a classical percolation model.[22] An average between the two fits gives a critical weight percent of $0.45 \pm 0.01\%$[4] and $0.015 \pm 0.005\%$ for the single-layer and bicomponent fibers, respectively.

When explaining the decreased critical weight percent in the core−sheath system, many factors must be taken into consideration. There are two mechanisms by which conducting paths across the sample may form in the mats. A conducting path may span the sample by connecting nanotubes in multiple fibers to create a single path, or many nanotubes within an individual fiber may result in a complete path. The main differences between the single and bicomponent fibers are an available volume reduction, less angular freedom for nanotubes, and a higher concentration of nanotubes close to the outer edge of the nanofiber. The volume reduction and angular distribution are related in that a smaller fiber diameter (or sheath confinement) directly leads to more aligned nanotubes. It has been shown that an increase in CNT alignment for homogeneous systems (homogeneous film, single fiber) leads to an increase in the threshold values.[29] Alignment effects become increasingly complex when looking at a heterogeneous system (e.g., a heterogeneous fiber placed randomly within a mat).[35] In the case of a fibrous mat, the nanotube angular distribution within each fiber is more constrained, but the fiber itself may take advantage of the entire space (be oriented over all angles). Thus, if the dominant mechanism is conduction within individual fibers, a high degree of MWNT alignment may exist. In contrast, if many fibers are involved in each path across the sample, then the MWNT could be considered randomly distributed. As to the volume reduction, ignoring it would roughly double (removing the previously mentioned division of 2) the critical weight percentage, which is still significantly below that of the single-layer fiber. In addition, with a greater concentration of nanotubes near the fiber surface, interfiber connections become more probable at lower weight percentages. Addressing the aggregation mentioned in the mechanical section, there are two points to be made. One, the aggregates became significant at a level above the critical weight percent. In this respect the effect of aggregates on the determination of the critical weight percent should be minimized. Second, aggregation of MWNTs can cause an increase in critical weight percent, but this only strengthens the argument for the core−sheath morphology. If aggregation is inflating the critical weight percent, then greater dispersion

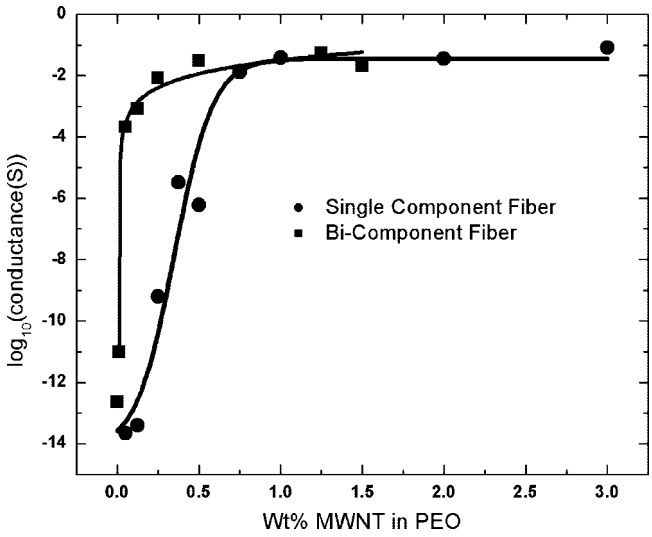

Figure 4. Conductance values for single-layer and bicomponent fibers. The wt % values for the bicomponent fiber were adjusted to reflect the wt % of the total fiber.

would only increase the difference between the single and bicomponent mats.

To better understand the mechanism by which the critical weight percentage is lowered for the core−sheath fibers, an ideal case will be investigated. For a single-layer fiber of diameter 200 nm containing MWNTs with an average diameter of 10 nm, the minimum volume percentage required for percolation *within* the fiber is the ratio of the nanotube and fiber cross-sectional areas, considering an ideal situation where the nanotubes are perfectly aligned end-to-end. This limiting case gives a weight percent of 0.27% for our physical system.

Measurements done by Wang et al.[28] for a single fiber show a critical weight percent of ∼0.5%, which is consistent with our previous results on single-component mats and is roughly double this minimum value. In contrast, core−sheath fibrous mats have a critical weight percent <1/10 of this ideal case. Even allowing for other factors (i.e., tunneling) would not bring down the minimum critical volume fraction to that of the core−sheath fibers. This simple thought experiment suggests that interfiber connections must contribute significantly to conductance along the mat. With that in mind, the greater concentration of nanotubes near the surface in the core−sheath geometry likely contributes to the lower critical weight percentage.

Conclusion

In the present work, electrospinning has been used as a facile technique to fabricate core−sheath nanofibers with pure PEO as core component and PEO doped with multiwalled carbon nanotubes as sheath component. Scanning electron microscopy has shown that nanofibers formed are similar to those of single-layer nanofibers. Core−sheath structure was verified by transmission electron microscopy. Conductivity measurements on fibrous mats have shown that the percolation threshold is significantly lower for the core−sheath morphology as compared to the single layer. In addition, the mechanical property data show that the bicomponent mats had an increased modulus with respect to the single-component fibers. In addition, the maximum mechanical strength occurred at a lower concentration in the bicomponent mats, indicating a lower threshold for nanotube aggregation.

Acknowledgment. Funding was provided by the NC State University Faculty Research and Professional Development Program.

References and Notes

(1) Iijima, S. *Nature (London)* **1991**, *6348*, 56–58.
(2) Baughman, R.; Zakhidov, A.; deHeer, W. *Science* **2002**, *5582*, 787–792.
(3) Collins, P.; Arnold, M.; Avouris, P. *Science* **2001**, *5517*, 706–709.
(4) McCullen, S. D.; Stevens, D. R.; Roberts, W. A.; Ojha, S. S.; Clarke, L. I.; Gorga, R. E. *Macromolecules* **2007**, *4*, 997–1003.
(5) Reneker, D. H.; Chun, I. *Nanotechnology* **1996**, *3*, 216–223.
(6) Vigolo, B.; Penicaud, A.; Coulon, C.; Sauder, C.; Pailler, R.; Journet, C.; Bernier, P.; Poulin, P. *Science* **2000**, *5495*, 1331–1334.
(7) Dalton, A. B.; Collins, S.; Munoz, E.; Razal, J. M.; Ebron, V. H.; Ferraris, J. P.; Coleman, J. N.; Kim, B. G.; Baughman, R. H. *Nature (London)* **2003**, *6941*, 703–703.
(8) Ko, F.; Khan, S.; Ali, A.; Gogotsi, Y.; Naguib, N.; Yang, G.; Li, C.; Shimoda, H.; Zhou, O.; Bronikowski, M. J.; Smalley, R. E.; Willis, P. A. *Proc. Am. Inst. Aeronautics Astronautics* **2002**, 1426.
(9) Ko, F.; Gogotsi, Y.; Ali, A.; Naguib, N.; Ye, H.; Yang, G.; Li, C.; Willis, P. *Adv. Mater.* **2003**, *15*, 1161–1165.
(10) Lam, H.; Titchenal, N.; Naguib, N.; Ye, H.; Gogotsi, Y.; Ko, F. *Mater. Res. Soc. Symp. Proc.* **2003**, *791*, Q10.5.1Q10.5.6.
(11) Dror, Y.; Salalha, W.; Khalfin, R. L.; Cohen, Y.; Yarin, A. L.; Zussman, E. *Langmuir* **2003**, *17*, 7012–7020.
(12) Formhals, A. U.S. Patent 1,975,504, **1934**.
(13) Bognitzki, M.; Czado, W.; Frese, T.; Schaper, A.; Hellwig, M.; Steinhart, M.; Greiner, A.; Wendorff, J. H. *Adv. Mater.* **2001**, *13*, 70–72.
(14) Jin, H.; Chen, J.; Karageorgiou, V.; Altman, G.; Kaplan, D. *Biomaterials* **2004**, *6*, 1039–1047.
(15) MacDiarmid, A. G.; Jones, W. E.; Norris, I. D.; Gao, J.; Johnson, A. T.; Pinto, N. J.; Hone, J.; Han, B.; Ko, F. K.; Okuzaki, H.; Llaguno, M. *Synth. Met.* **2001**, *1*, 27–30.
(16) Kim, C.; Yang, K. S. *Appl. Phys. Lett.* **2003**, *6*, 1216–1218.
(17) Drew, C.; Liu, X.; Ziegler, D.; Wang, X.; Bruno, F. F.; Whitten, J.; Samuelson, L. A.; Kumar, J. *Nano Lett.* **2003**, *2*, 143–147.
(18) Tsai, P.; Schreuder-Gibson, H.; Gibson, P. *J. Electrost.* **2002**, *3*, 333–341.
(19) Shao, C.; Kim, H.; Gong, J.; Ding, B.; Lee, D.; Park, S. *Mater. Lett.* **2003**, *9*, 1579–1584.
(20) Kenawy, E.; Bowlin, G.; Mansfield, K.; Layman, J.; Simpson, D.; Sanders, E.; Wnek, G. *J. Controlled Release* **2002**, *1*, 57–64.
(21) Zhang, Y.; Huang, Z.; Xu, X.; Lim, C. T.; Ramakrishna, S. *Chem. Mater.* **2004**, *18*, 3406–3409.
(22) Stauffer, D.; Aharony, A. *Introduction to Percolation Theory*; Taylor & Francis: Washington, DC, 1992.
(23) Sundaray, B.; Subramanian, V.; Natarajan, T. S. K. *Appl. Phys. Lett.* **2006**, *14*, 143114.
(24) Coleman, J. N.; Curran, S.; Dalton, A. B.; Davey, A. P. *Phys. Rev. B* **1998**, *12*, R7492–R7495.
(25) Barrau, S.; Demont, P.; Peigney, A.; Laurent, C.; Lacabanne, C. *Macromolecules* **2003**, *14*, 5187–5194.
(26) Sandler, J. K. W.; Kirk, J. E.; Kinloch, I. A.; Shaffer, M. S. P.; Windle, A. H. *Polymer* **2003**, *19*, 5893–5899.
(27) McLachlan, D. S.; Chiteme, C.; Park, C.; Wise, J. *J. Polym. Sci., Part B: Polym. Phys.* **2005**, 3273–3287.
(28) Wang, G.; Tan, Z.; Liu, X.; Chawda, S.; Koo, J. *Nanotechnology* **2006**, *23*, 5829–5835.
(29) Natsuki, T.; Endo, M.; Takahashi, T *Physica A* **2005**, *2*, 498–508.
(30) Du, F.; Fischer, J. E.; Winey, K. I. *Phys. Rev. B* **2005**, *12*, 121404.
(31) Sun, Z.; Zussman, E.; Yarin, A. L.; Wendorff, J. H.; Greiner, A. *Adv. Mater.* **2003**, 1929–1932.
(32) Ren, Z. F.; Huang, Z. P.; Xu, J. W.; Wang, J. H.; Bush, P.; Siegal, M. P.; Provencio, P. N. *Science* **1998**, *5391*, 1105–1107.
(33) Van Gerwen, P.; Laureyn, W.; Laureys, W.; Huyberechts, G. *Sens. Actuators, B* **1998**, 73–80.
(34) Fournier, J.; Boiteux, G.; Seytre, G.; Marichy, G. *Synth. Met.* **1997**, *1*, 839–840.
(35) Du, F.; Cuthy, C.; Kashiwagi, T.; Fischer, J. E. *J. Polym. Sci., Part B: Polym. Phys.* **2006**, *44*, 1513–1519.

MA702634A